Optically Addressing Single Rare-Earth Ions in a Nanophotonic Cavity

Tian Zhong,[1,2,3,*] Jonathan M. Kindem,[1,2] John G. Bartholomew,[1,2] Jake Rochman,[1,2] Ioana Craiciu,[1,2] Varun Verma,[4] Sae Woo Nam,[4] Francesco Marsili,[5] Matthew D. Shaw,[5] Andrew D. Beyer,[5] and Andrei Faraon[1,2,†]

[1]*Kavli Nanoscience Institute and Thomas J. Watson, Sr., Laboratory of Applied Physics, California Institute of Technology, Pasadena, California 91125, USA*

[2]*Institute for Quantum Information and Matter, California Institute of Technology, Pasadena, California 91125, USA*

[3]*Institute for Molecular Engineering, University of Chicago, Chicago, Illinois 60637, USA*

[4]*National Institute of Standards and Technology, 325 Broadway, MC 815.04, Boulder, Colorado 80305, USA*

[5]*Jet Propulsion Laboratory, California Institute of Technology, 4800 Oak Grove Drive, Pasadena, California 91109, USA*

(Received 20 March 2018; published 31 October 2018)

We demonstrate optical probing of spectrally resolved single Nd^{3+} rare-earth ions in yttrium orthovanadate. The ions are coupled to a photonic crystal resonator and show strong enhancement of the optical emission rate via the Purcell effect, resulting in near radiatively limited single photon emission. The measured high coupling cooperativity between a single photon and the ion allows for the observation of coherent optical Rabi oscillations. This could enable optically controlled spin qubits, quantum logic gates, and spin-photon interfaces for future quantum networks.

DOI: 10.1103/PhysRevLett.121.183603

Rare-earth dopants in solids exhibit long-lived coherence in both the optical and spin degrees of freedom [1,2]. The effective shielding of $4f$ electrons leads to optical and radio frequency transitions with less sensitivity to noise in their crystalline surroundings at cryogenic temperatures. Significant progress in rare-earth-based quantum technologies has led to ensemble-based optical quantum memories [3–6] and coherent transducers [7], with promising performance as quantum light-matter interfaces for quantum networks. On the other hand, addressing single ions has remained an outstanding challenge, with the progress hindered by the long optical lifetimes of rare-earth ions and resultant faint photoluminescence (PL). So far, only a few experiments have succeeded in isolating individual praseodymium [8–10], cerium [11–13], and erbium [14,15] ions, though the majority of them did not probe ions via their $4f$-$4f$ optical transitions. Recently, several works have demonstrated significant enhancement of spontaneous emission of rare-earth emitters coupled to a nanophotonic cavity [6,15–17], among which [6,16] also showed negligible detrimental effect on the coherence properties of ions in nanodevices. These results point at a viable approach to efficiently detect and coherently control individual ions in a chip-scale architecture.

Here we demonstrate a nanophotonic platform based on a yttrium orthovanadate (YVO_4) photonic crystal nanobeam resonator coupled to spectrally resolved individual neodymium (Nd^{3+}) ions. While the system acts as an ensemble quantum memory when operating at the center of the inhomogeneous line [6], it also enables direct optical addressing of single Nd^{3+} in the tails of the inhomogeneous distribution, which show strongly enhanced, near radiatively limited, single photon emission. A measured vacuum Rabi frequency of $2\pi \times 28.5$ MHz significantly exceeds the linewidth of a Nd^{3+} ion, allowing for coherent manipulation of spins with optical pulses. Unlike prior experiments [8–13], this technique does not hinge on the spectroscopic details of a specific type of ion and can be readily extended to other rare earths or defect centers. The technique opens up new opportunities for spectroscopy on single ions that are distinct from conventional ensemble measurements, which enables probes for the local nanoscopic environment around individual ions and may lead to new quantum information processing, interconnect, and sensing devices.

Our experiment builds upon a triangular nanobeam photonic crystal resonator [16,18] that was fabricated in a nominally 50 ppm doped $Nd^{3+}:YVO_4$ crystal using focused ion beam (FIB) milling [18]. The device is a one-sided cavity, as the input [left mirror in Figs. 1(a) and 1(b)] has a lower reflectivity. The optical coupling in and out of the device was implemented via a 45°-angled coupler [16]. An aspheric doublet mode matches the single-mode fiber to the nanobeam waveguide [Fig. 1(a)]. The coupling efficiency was optimized to 19% (from fiber to waveguide) using a three-axis nanopositioner. The nanocavity fundamental mode volume is $V_{\mathrm{mode}} = 0.056\ \mu\mathrm{m}^3$ (simulated) with a measured quality factor $Q = 3900$ (energy decay rate $\kappa = 2\pi \times 90$ GHz). The waveguide-cavity coupling κ_{in} through the input mirror was 45% of κ. The device was cooled to ~20 mK base temperature in a dilution refrigerator, though the actual ensemble temperature was estimated to be around 500 mK (by comparing the ground Zeeman level populations from the PL spectra). The elevated temperature was attributed to the very small

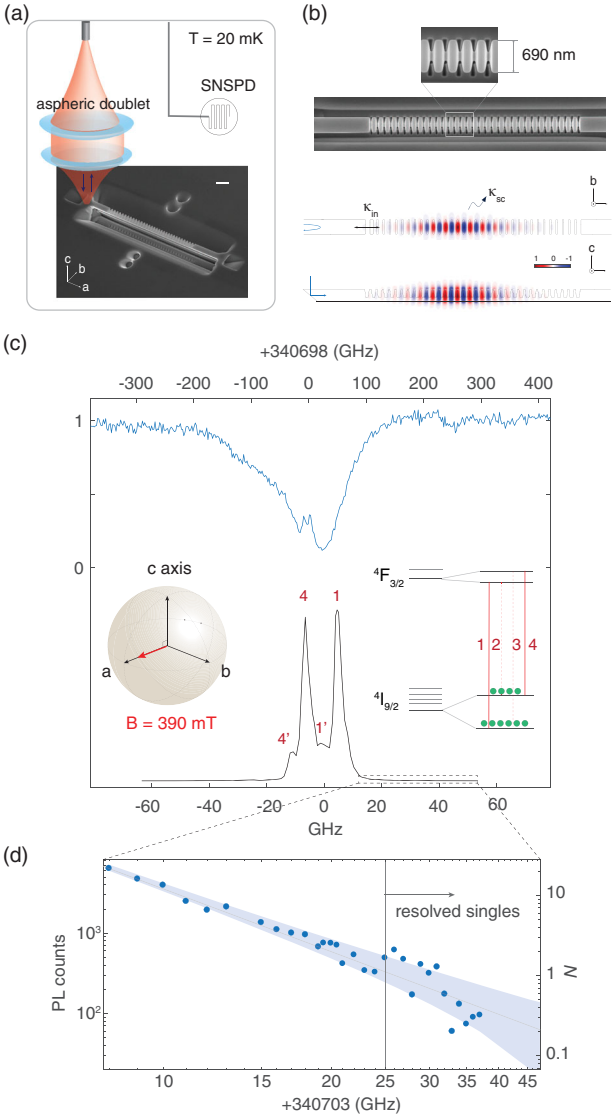

FIG. 1. (a) Schematics of the experiment in a dilution refrigerator. Scale bar is 1 μm. (b) SEM images of the one-sided nanobeam photonic crystal cavity in YVO_4 fabricated using FIB. The Lower part shows the simulated TM fundamental mode profile, which has the polarization aligned to the dipoles of Nd^{3+} along the crystallographic c axis. (c) Cavity reflection spectrum (upper) and Nd^{3+} photoluminescence spectrum (lower). (Insets) Applied magnetic field and resulting Zeeman levels and transitions. PL from ions in the bulk substrate (1' and 4') appear redshifted from ions coupled to the cavity (1 and 4). (d) Atomic spectra density versus detuning on the shorter wavelength tail of the inhomogeneous distribution. The shaded area shows the projected atomic shot noise.

thermal conductance in the nanobeam. This limitation has already manifested in previous sub-Kelvin bulk sample measurements [19] and was even more demanding for measuring nanodevices in the current case. The laser for probing the ions was modulated by two double-pass acousto-optic modulators and delivered to the sample via a single-mode fiber. The reflected signal from the device was sent via a circulator to a superconducting nanowire single photon detector (SNSPD) that measured a 82% detection efficiency at 880 nm and < 2 Hz dark counts [6]. The SNSPD was mounted in the same fridge at the 100 mK stage. The overall photon detection efficiency including transmission from the cavity to the detector and the detector efficiency was 3.6% (see Supplemental Material [20]).

A typical cavity reflection spectrum when tuned nearly on resonance with the Nd^{3+} ${}^4F_{3/2}(Y_1) - {}^4I_{9/2}(Z_1)$ transition at 880 nm is shown in Fig. 1(c). A 390 mT magnetic field was applied along the crystallographic a axis of YVO_4, giving rise to split Zeeman levels and four possible optical transitions [34] (labeled 1–4) shown in the inset. Symmetry considerations impose that the 2, 3 cross transitions are forbidden and the 1, 4 transitions are close to cyclic [6,35]. The PL spectrum (with a 200-ns pulsed resonant excitation) is shown in the lower part of Fig. 1(c). Two weak lines labeled 1' and 4' were identified as emissions from Nd^{3+} ions in the bulk substrate, which are red detuned from ions coupled to the cavity by 2.5 GHz. This shift is due to a static strain in the nanobeam, which makes it easier to spectrally separate the ions in the cavity from the bulk. For subsequent experiments, we focus on the shorter wavelength tail of the inhomogeneous distribution. Figure 1(d) plots the resonant PL against detuning from the peak of line 1 (340 703.0 GHz). The PL and thus the atomic spectral density (N ions per excitation pulse bandwidth) fits with a power law of $N \propto \Delta^{-2.9}$, where Δ is the detuning. The 2.9 power exponent indicates an inhomogeneous broadening mechanism due to strain by dislocation, according to the asymptotic form in [37]. Statistical fine structure (SFS) [38] was also evident. By fitting the SFS with the projected shot noise of N ($\sqrt{N}$ indicated as the shaded area), it is projected that discrete single ion spectra ($N < 1$) emerge at a detuning > 25 GHz.

To search for singles, we scanned the frequency of a 200-ns resonant excitation pulse around ~30 GHz blue detuning from the peak of line 1 and measured the PL integrated over 5 μs after the excitation. The repetition rate of the excitation pulses was 25 kHz, and the integration time was 20 s at each frequency. The laser was frequency stabilized to a vacuum-chamber reference cavity, attaining a narrowed linewidth of < 5 kHz and a long-term drift < 100 kHz/day. Figure 2(a) shows the measured PL over a few gigahertz range. A handful of peaks, such as the one with the close-up in Fig. 2(c), were possible single Nd^{3+} ions. The PL intensities were histogrammed in Fig. 2(b) to reveal a distribution of ion-cavity coupling strengths, which is in good agreement with that from the finite difference time domain (FDTD) simulation (red). Thus, the PL intensity serves to correlate the coupling strength of each ion with its spatial position relative to the cavity antinodes: an ion located at the antinode would have the strongest coupling and show the highest PL. The linewidth of the peak in Fig. 2(c) was broadened by the excitation pulse. The actual linewidth of single ions was

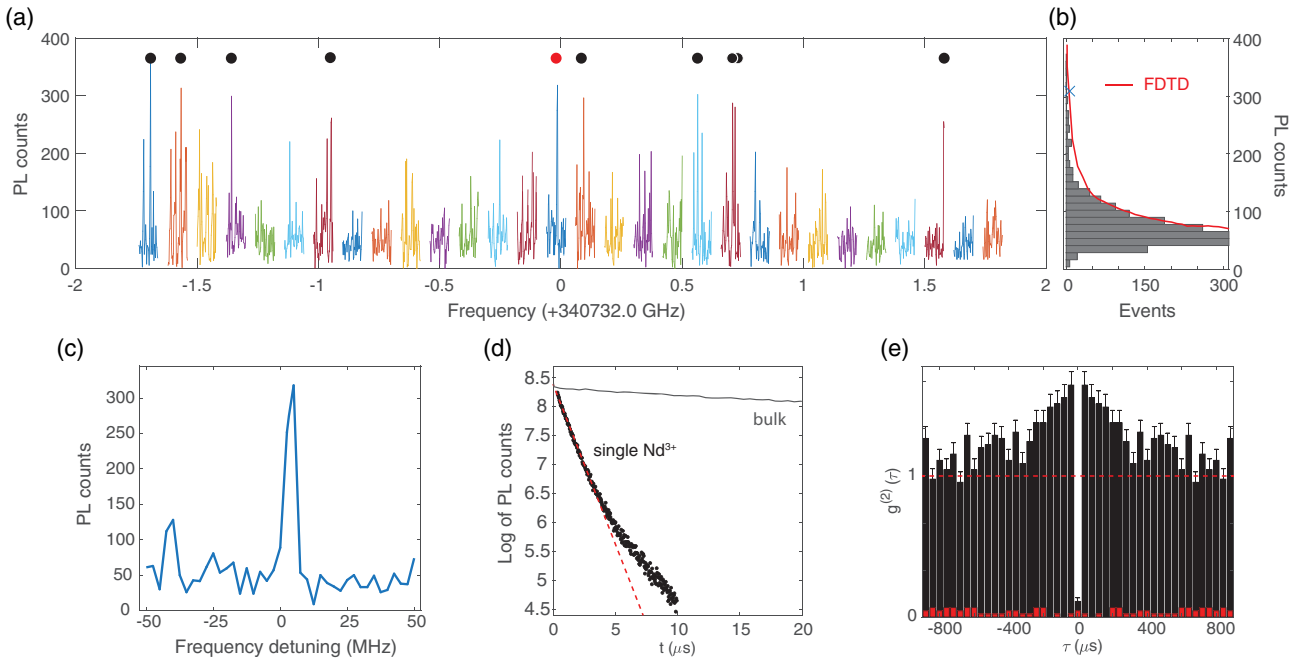

FIG. 2. (a) Photoluminescence spectrum swept over 3 GHz around $\Delta \sim 30$ GHz. Isolated peaks marked by filled circles correspond to individual Nd^{3+} ions. Each color represents a different laser scan. (b) Histogram of PL intensities from the ensemble of Nd^{3+}. The red curve is a FDTD simulation of the expected distribution given the different position of each ion inside the cavity. (c) PL spectrum of the ion labeled with the red circle in Fig. 2(a). (d) PL decay of the ion (black) with a fitted $T_1 = 2.1 \pm 0.2$ μs (red) compared to $T_1 = 90$ μs in bulk (gray). (e) Intensity autocorrelation measurement on the single Nd^{3+} showing antibunching [$g^2(0) = 0.09 \pm 0.013$]. The background signal with an off-resonant excitation is in red.

expected to be considerably narrower. With the laser tuned on resonance with one of the peaks [marked with a red dot in Fig. 2(a)], the intensity autocorrelation measurement using a single detector yielded a $g^{(2)}(0) = 0.09 \pm 0.013$ [Fig. 2(e)] with ~0.02 photons generated per pulse, which was normalized to $g^{(2)}(t)$ at large τ. The bunching behavior at $|\tau| < 600$ μs was expected from a multilevel emitter [39,40]. The imperfect antibunching was partly due to a continuum of ions that is weakly coupled to the cavity, resulting in a background in Fig. 2(e). This background was measured with the excitation laser far detuned from the single ion resonance. The optical T_1 of this ion was 2.1 ± 0.2 μs [Fig. 2(d)], which is strongly enhanced compared to the bulk T_1 of 90 μs. The lifetime enhancement corresponded to a Purcell factor of 111 of the probed Y_1-Z_1 transition considering a branching ratio of $\beta = 0.38$ (the ground state splits into five Kramers doublets Z_1-Z_5) [20]. The theoretically maximum Purcell factor was $F \approx (3/4\pi^2\chi_L^2)(\lambda/n_{YVO_4})^3(Q/V) = 189$ [26,41], assuming a perfect alignment of the dipole with the cavity mode and $\chi_L = 3n_{YVO_4}^2/(2n_{YVO_4}^2 + 1)$ is the local correction to the electric field since the ion is less polarizable than the bulk medium [25], where we have used the real cavity approximation (see Supplemental Material [20]). The discrepancy is attributed to the nonoptimal position of the ion, and the actual cavity mode volume being different from simulation because of fabrication imperfections.

The small mode volume of the nanocavity results in a significant enhancement of the coupling strength g_0. Focusing on the ion in Fig. 2(c), Fig. 3(a) plots the PL excited by a square 250-ns resonant pulse with increasing cavity mean photon number $\bar{n}$. The value of $\bar{n}$ was calculated from the input pulse energy, all losses in the setup up to the device, and coupling rates of the photonic crystal mirrors (see Supplemental Material [20]). The PL shows Rabi oscillations similar to an optical nutation [42]. The inset plots the extracted Rabi frequencies Ω versus square root of $\bar{n}$ from the peaks (corresponding to an odd integer of π pulse areas) and valleys (even integer of π pulses) of the Rabi oscillations. The fitted slope corresponds to $g_0 = \Omega/2\sqrt{\bar{n}} = 2\pi \times 28.5 \pm 5.2$ MHz. The theoretical maximum g_0 is $\mu/n_{YVO_4}\sqrt{\omega_0/2\hbar\epsilon_0 V} = 2\pi \times 52.7$ MHz [26], where $\mu = 1.59 \times 10^{-31}$ C m is the transition dipole moment (see Supplemental Material [20]), $n_{YVO_4} = 2.1785$ is the refractive index of YVO_4, ω_0 is the transition frequency, and ϵ_0 is the vacuum permittivity. The measured g_0 is orders of magnitude larger than the linewidth of the emitter, which makes possible the use of hard optical pulses [43] to coherently control each single ion. Next, we applied two $\pi/2$ pulses to measure the Ramsey interference as shown in Fig. 3(b). The normalized Ramsey fringes (subtracting a T_1 decay background) reveal a clear beating, which most likely corresponds to the superhyperfine interactions between the Nd electron spins

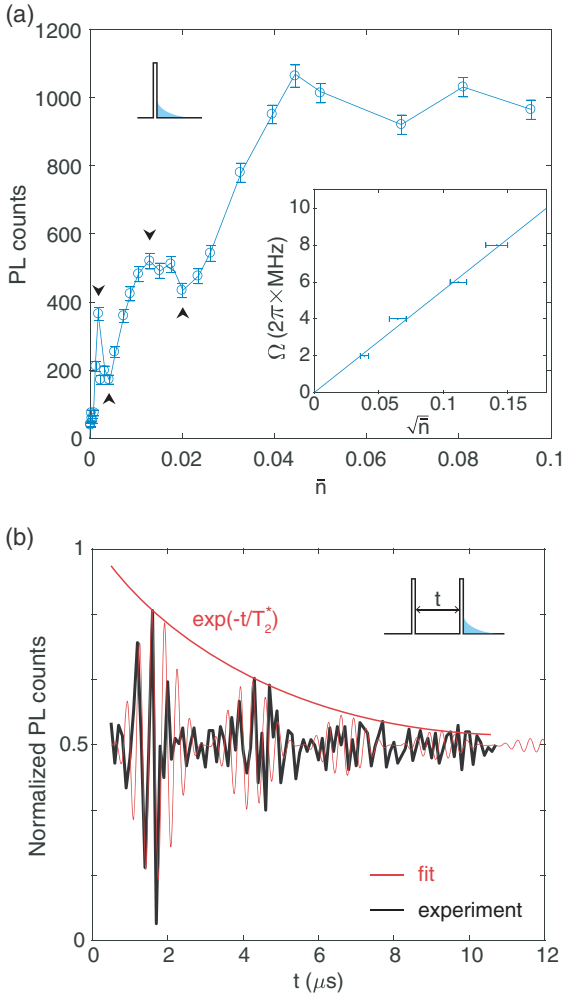

FIG. 3. (a) Rabi oscillations of PL following a pulsed resonant excitation with increasing photon number $\bar{n}$. Black arrows point to pulse areas that are integer multiples of π. (Inset) Extracted Rabi frequencies against $\sqrt{\bar{n}}$ with a linear fit. (b) Normalized Ramsey interference fringes. The beating at a frequency of 740 kHz is consistent with the superhyperfine coupling between the Nd^{3+} ion and surrounding Y.

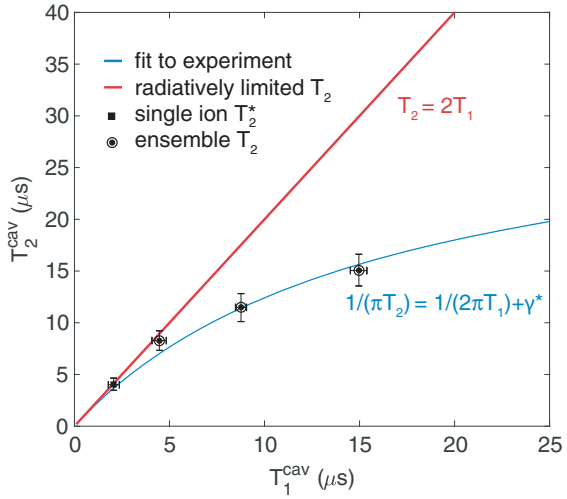

FIG. 4. Measured and theoretical optical coherences for Nd^{3+} coupled to the cavity with varying detuning and Purcell enhancement. The red line is the radiatively limited T_2 time. The single Nd^{3+} on resonance with the cavity (square) exhibits a near radiatively limited linewidth with a spectral indistinguishability $> 95\%$.

and the nuclear spins of yttrium in YVO_4 [20]. The measured superhyperfine beating, confirmed by the two-pulse photon echo measurement (see Supplemental Material [20]), was 740 kHz, which is consistent with the calculations based on the gyromagnetic ratio of yttrium (Y) nuclear spins of ~2.1 MHz/T [20,30]. At a relatively strong field of 390 mT, the Nd-Y superhyperfine structure is dominated by the yttrium nuclear magnetic moment (Supplemental Material [20]), as also observed in $Nd^{3+}:Y_2SiO_5$ [29]. The decay of the Ramsey fringe envelope can be fitted empirically to extract a $T_2^* = 4.0 \pm 0.2$ μs. From that, the spectral indistinguishability is calculated as $T_2/(2T_1) = 0.952$, indicating that the linewidth of this ion approaches the radiatively limited regime.

The use of single rare-earth ions as spin-photon interfaces to entangle remote quantum nodes requires each emitter's linewidth to be radiatively limited. To further characterize the coherence of the ions coupled to the cavity, we performed additional ensemble two-pulse photon echo measurements when the emitters have different detunings from cavity resonance. The ensemble T_2 times are plotted against optical T_1 in Fig. 4, including the single ion T_2^* data denoted by a square. The experimental data were fitted with the relationship $1/(\pi T_2) = 1/(2\pi T_1) + \gamma^*$, where γ^* is the pure dephasing rate. The fit (blue curve) gives a $\gamma^* = 9.7 \pm 0.6$ kHz. While slow, this dephasing rate was attributed to the superhyperfine interactions since it closely matches the superhyperfine-limited T_2 in $Nd^{3+}:YVO_4$ [2]. The contribution from Nd^{3+} spin flip-flops are expected to be small, because the measured T_2 in an nominally undoped YVO_4 crystal (residual doping estimated at 0.2 ppm) was comparable to that measured in the current device (see Supplemental Material [20]).

The full radiatively limited $T_2 = 2T_1$ is plotted in red. With weak enhancement when the ions are detuned from the cavity, the ions exhibit poor indistinguishabilities, as indicated by the sizable gap between the red and blue curves. Only when the ions are resonantly coupled to the cavity do they become radiatively limited. A similar approach has been used to improve the single photon indistinguishabilities of quantum dots [44]. To increase the indistinguishability, improving the cavity quality factor to further reduce T_1 would be a straightforward step, which would also allow the device to operate at higher temperatures with stronger dephasing while still achieving radiatively limited emission. The current linewidth of the single emitter was based on T_2^* values measured over a few microseconds [Fig. 3(b)]. For longer timescales (100 μs to

ms), reducing the slow optical spectral diffusion could help to maintain a high indistinguishability, as desired by quantum memories for long-distance quantum network. In that regard, using rare-earth emitters in hosts with weaker nuclear spin baths or non-Kramers ions with weaker superhyperfine couplings and operating at a zero-first-order-Zeeman point [45] may offer some advantages.

In conclusion, we have optically detected single Nd^{3+} ions coupled to a nanophotonic cavity, which enhanced the emitter spontaneous emission rate to the extent that the linewidth of the emitter became radiatively limited. Optical Rabi oscillations of the single Nd^{3+} yielded a $g_0 = 2\pi \times 28.5$ MHz and a linewidth of 12.5 kHz $[\gamma_h = 1/(\pi T_2)]$, where $T_2 = 25.4\ \mu$s is the emitter homogeneous linewidth without cavity enhancement (see Supplemental Material [20]). Given the cavity decay of $\kappa = 2\pi \times 90$ GHz, the single ion cooperativity is $4g_0^2/\kappa\gamma_h = 2.9$. This value could be improved significantly by using cavities with higher Q ($\times 10$ higher Q devices already demonstrated in [18] would attain an indistinguishability $> 99.5\%$ and $C \sim 30$), thus making feasible the implementation of high-fidelity non-destructive detection of optical photons with a single rare-earth ion [46]. Nevertheless, questions remain regarding the spin coherence and the qubit storage time of single ions [47] and spectral diffusion occurring at longer timescales. When two spectrally resolved ions are nearby, their dipole-dipole interaction can also be probed [48]. Single rare-earth ions could be used to probe the field and temperature of its nanoscopic surroundings. Finally, the large inhomogeneous linewidth of the emitters may facilitate spectral multiplexing of individual quantum emitters for expanded bandwidth of quantum communication networks.

This work was funded by a National Science Foundation (NSF) Faculty Early Career Development Program (CAREER) Grant (No. 1454607), the AFOSR Quantum Transduction Multidisciplinary University Research Initiative (FA9550-15-1-002), and the Defense Advanced Research Projects Agency Quiness program (W31P4Q-15-1-0012). Equipment funding was also provided by the Institute of Quantum Information and Matter, an NSF Physics Frontiers Center with support from the Moore Foundation. The device nanofabrication was performed in the Kavli Nanoscience Institute at the California Institute of Technology. Part of the research was carried out at the Jet Propulsion Laboratory, California Institute of Technology, under a contract with the National Aeronautics and Space Administration. The authors would like to acknowledge Neil Sinclair, Ruffin Evans, Alp Sipahigil, Charles W. Thiel, and Jeffrey Thompson for useful discussions.

*tzh@uchicago.edu
†faraon@caltech.edu

[1] C. W. Thiel, T. Böttger, and R. L. Cone, J. Lumin. **131**, 353 (2011).
[2] Y. Sun, C. W. Thiel, R. L. Cone, R. W. Equall, and R. L. Hutcheson, J. Lumin. **98**, 281 (2002).
[3] W. Tittel, M. Afzelius, T. Chaneliére, R. L. Cone, S. Kröll, S. A. Moiseev, and M. Sellars, Laser Photonics Rev. **4**, 244 (2010).
[4] H. de Riedmatten, M. Afzelius, M. U. Staudt, C. Simon, and N. Gisin, Nature (London) **456**, 773 (2008).
[5] M. P. Hedges, J. J. Longdell, Y. Li, and M. J. Sellars, Nature (London) **465**, 1052 (2010).
[6] T. Zhong *et al.*, Science **357**, 1392 (2017).
[7] L. A. Williamson, Y.-H. Chen, and J. J. Longdell, Phys. Rev. Lett. **113**, 203601 (2014).
[8] R. Kolesov, K. Xia, R. Reuter, R. Stöhr, A. Zappe, J. Meijer, P. R. Hemmer, and J. Wrachtrup, Nat. Commun. **3**, 1029 (2012).
[9] T. Utikal, E. Eichhammer, L. Petersen, A. Renn, S. Götzinger, and V. Sandoghdar, Nat. Commun. **5**, 3627 (2014).
[10] I. Nakamura, T. Yoshihiro, H. Inagawa, S. Fujiyoshi, and M. Matsushita, Sci. Rep. **4**, 7364 (2014).
[11] R. Kolesov, K. Xia, R. Reuter, M. Jamali, R. Stöhr, T. Inal, P. Siyushev, and J. Wrachtrup, Phys. Rev. Lett. **111**, 120502 (2013).
[12] P. Siyushev *et al.*, Nat. Commun. **5**, 3895 (2014).
[13] K. Xia *et al.*, Phys. Rev. Lett. **115**, 093602 (2015).
[14] C. Yin, M. Rancic, G. G. de Boo, N. Stavrias, J. C. McCallum, M. J. Sellars, and S. Rogge, Nature (London) **497**, 91 (2013).
[15] A. M. Dibos, M. Raha, C. M. Phenicie, and J. D. Thompson, Phys. Rev. Lett. **120**, 243601 (2018).
[16] T. Zhong, J. M. Kindem, E. Miyazono, and A. Faraon, Nat. Commun. **6**, 8206 (2015).
[17] T. Zhong, J. M. Kindem, J. Rochman, and A. Faraon, Nat. Commun. **8**, 14107 (2017).
[18] T. Zhong, J. Rochman, J. M. Kindem, E. Miyazono, and A. Faraon, Opt. Express **24**, 536 (2016).
[19] N. Kukharchyk, D. Sholokhov, O. Morozov, S. L. Korableva, A. A. Kalachev, and P. Bushev, New J. Phys. **20**, 023044 (2018).
[20] See Supplemental Material at http://link.aps.org/supplemental/10.1103/PhysRevLett.121.183603 for details about the experimental setup, optical spectroscopy and decoherence studies of $Nd^{3+}:YVO_4$, which includes Ref. [21–36].
[21] T. G. Tiecke, K. P. Nayak, J. D. Thompson, T. Peyronel, N. P. de Leon, V. Vuletić, and M. D. Lukin, Optica **2**, 70 (2015).
[22] B. Di Bartolo, *Optical Interactions in Solids* (Wiley, New York, 1968).
[23] B. Henderson and G. Imbush, *Optical Spectroscopy of Inorganic Solids* (Oxford University Press, Oxford, 2006).
[24] K. Dolgaleva and R. W. Boyd, Adv. Opt. Photonics **4**, 1 (2012).
[25] H. T. Dung, S. Y. Buhmann, and D.-G. Welsch, Phys. Rev. A **74**, 023803 (2006).
[26] D. L. McAuslan, J. J. Longdell, and M. J. Sellars, Phys. Rev. A **80**, 062307 (2009).
[27] M. F. Reid, in *Spectroscopic Properties of Rare Earths in Optical Materials*, edited by G. Liu and B. Jacquier (Springer, Berlin, 2005).

[28] P. de Vries and A. Lagendijk, Phys. Rev. Lett. **81**, 1381 (1998).
[29] I. Usmani, M. Afzelius, H. de Riedmatten, and N. Gisin, Nat. Commun. **1**, 12 (2010).
[30] B. Car, L. Veissier, A. Louchet-Chauvet, J.-L. Le Gouët, and T. Chanelière, Phys. Rev. Lett. **120**, 197401 (2018).
[31] W. B. Mims, Phys. Rev. B **5**, 2409 (1972).
[32] H. de Riedmatten, M. Afzelius, M. U. Staudt, C. Simon, and N Gisin, Nature (London) **456**, 773 (2008).
[33] T. Böttger, C. W. Thiel, Y. Sun, and R. L. Cone, Phys. Rev. B **73**, 075101 (2006).
[34] S. R. Hastings-Simon *et al.*, Phys. Rev. B **77**, 125111 (2008).
[35] M. Afzelius, M. U. Staudt, H. de Riedmatten, N. Gisin, O. Guillot-Noël, P. Goldner, R. Marino, P. Porcher, E. Cavalli, and M. Bettinelli, J. Lumin. **130**, 1566 (2010).
[36] T. Böttger, C. W. Thiel, R. L. Cone, and Y. Sun, Phys. Rev. B **79**, 115104 (2009).
[37] A. M. Stoneham, Rev. Mod. Phys. **41**, 82 (1969).
[38] W. E. Moerner and T. P. Carter, Phys. Rev. Lett. **59**, 2705 (1987).
[39] C. Kurtsiefer, S. Mayer, P. Zarda, and H. Weinfurter, Phys. Rev. Lett. **85**, 290 (2000).
[40] E. Wu, V. Jacques, H. Zeng, P. Grangier, F. Treussart, and J.-F. Roch, Opt. Express **14**, 1296 (2006).
[41] E. M. Purcell, Phys. Rev. **69**, 681 (1946).
[42] I. Gerhardt, G. Wrigge, G. Zumofen, J. Hwang, A. Renn, and V. Sandoghdar, Phys. Rev. A **79**, 011402(R) (2009).
[43] G. J. Pryde, M. J. Sellars, and N. B. Manson, Phys. Rev. Lett. **84**, 1152 (2000).
[44] T. Grange, N. Somaschi, C. Antón, L. De Santis, G. Coppola, V. Giesz, A. Lemaître, I. Sagnes, A. Auffèves, and P. Senellart, Phys. Rev. Lett. **118**, 253602 (2017).
[45] E. Fraval, M. J. Sellars, and J. J. Longdell, Phys. Rev. Lett. **92**, 077601 (2004).
[46] C. O'Brien, T. Zhong, A. Faraon, and C. Simon, Phys. Rev. A **94**, 043807 (2016).
[47] G. Wolfowicz, H. Maier-Flaig, R. Marino, A. Ferrier, H.é Vezin, J. J. L. Morton, and P. Goldner, Phys. Rev. Lett. **114**, 170503 (2015).
[48] J. J. Longdell and M. J. Sellars, Phys. Rev. A **69**, 032307 (2004).